IEEE Access
Multidisciplinary | Rapid Review | Open Access Journal

Received November 6, 2019, accepted November 21, 2019, date of publication December 4, 2019,
date of current version December 19, 2019.

Digital Object Identifier 10.1109/ACCESS.2019.2957493

A Single Receive Channel DBF Method for Ultra-Wideband Radar

LIU NAN, GUO KAISI, ZHANG ZHENGHE, AND ZHANG LINRANG
National Laboratory of Radar Signal Processing, Xidian University, Xi'an 710071, China

Corresponding author: Liu Nan (liunaneoe@163.com)

This work was supported in part by the National Natural Science Foundation of China under Grant 61731023 and Grant 61671361.

ABSTRACT In this paper, we present a space code agility-based single receive channel digital beamforming (DBF) method for ultra-wideband radar. The proposed single channel DBF method outperforms the existing single channel DBF method with a space-time coded array architecture regarding both the angular and the range sidelobe levels by integrating multiple pulses modulated by irrelevant space codes. A frequency-domain equivalent DBF algorithm is also developed. This algorithm is immune to the mismatch between the sampling rate of the recorded signal and the space-time response function of the space-time coded array under ultra-wideband circumstances, in which cases the existing space-time coded array DBF methods will suffer. Moreover, the target motion over multiple pulse repetition intervals (PRIs) is taken into account in the development of the frequency-domain DBF algorithm. Therefore, performance degradation due to target motion is avoided. Numerical simulations verify the effectiveness of the proposed method.

INDEX TERMS Digital beamforming (DBF), single receive channel, ultra-wideband radar, space-time coded array, space code agility.

I. INTRODUCTION

The digital beamforming (DBF) technique has been widely studied in the last few decades since it outperforms the analog beamforming technique in many aspects [1]. However, the DBF technique must employ an independent radio frequency (RF) receive channel for each array element or subarray; as a result, the hardware of the antenna system is expensive. Moreover, the DBF performance will suffer from errors between the receive channels. Therefore, over the past decade, low-cost single-channel DBF methods have been developed.

By sequentially connecting a single RF receive channel to different array elements, the spatial multiplexing of local elements (SMILE) method [2]–[6] can recover the spatial samples of the array from the time-domain sample sequence. However, the recovered spatial samples are not recorded at the same time. Therefore, this approach requires a more complex DBF processing procedure. This problem can be resolved by introducing true-time delay (TTD) lines with different delay times [7]. However, the SMILE method requires a sampling rate much larger than the signal bandwidth such that the original signal can be fully recorded. In an ultra-wideband case, the available sampling rate of the analog to digital converter (ADC) may not meet this requirement, even if a small number of elements are utilized. The time sequence phase weighting (TSPW) method proposed in Ref. [8]–[11] can also realize DBF with a single receive channel. This method is essentially based on the spectrum spread technique. The received signals of array elements are modulated by orthogonal codes. Therefore, one can recover the received signals of the expected element by dispreading processing. The recovered spatial samples of TSPW will be obtained at the same sampling time. However, TSPW also requires a sampling rate much larger than the signal bandwidth, which will limit its application in ultra-wideband cases. In Ref. [12], another single receive channel DBF method was developed based on the circulating time-delay coded array (CTDCA) [13]–[15]. Compared to the method proposed in Ref. [7], this CTDCA-based method also introduces an increasing time delay across the array elements through TTD lines. The delayed signals are then summed together and fed to the single receiver. DBF can be accomplished through time-domain filtering if the time delay between any two neighboring elements equals the reciprocal of the signal bandwidth. This method still works even if the

The associate editor coordinating the review of this manuscript and approving it for publication was Huawei Chen.

sampling rate of the ADC is slightly larger than the signal bandwidth, which facilitates its application in ultra-wideband cases. Moreover, in ultra-wideband cases, shorter TTD lines are required, which also facilitates the implementation of a CTDCA in practice. However, such a method will result in a decrease in the range resolution. The range resolution can be preserved by further introducing space coding into the circulating time-delay coded array [16]. Such a technique, which has been developed for transmit beamforming, can also be utilized for single channel receive DBF. However the space coding technique will result in increases in the sidelobe levels in both the range domain and the angular domain. A subarray-based space-time coded array (STCA) was proposed in Ref. [17] to reduce the sidelobe levels. However, such STCA approach will result in a reduced spatial coverage. Furthermore, the methods mentioned above employ time-domain convolution to accomplish receive DBF. In ultra-wideband cases, time-domain convolution based DBF will suffer from a mismatch between the sampling rate of the recorded signal and the CTDCA system response function.

In this paper, we present a space code agility-based single receive channel DBF method for ultra-wideband radar. Under the proposed architecture of a single receive channel STCA, the received signals of multiple pulse repetition intervals (PRIs) will be utilized for DBF. The space code will vary from PRI to PRI. After coherently integrating the received signals of multiple PRIs, the relative sidelobe levels in both the range domain and the angular domain will be decreased compared to those in the existing single channel DBF methods with an STCA architecture. Furthermore, equivalent DBF processing is carried out in the frequency domain instead of the time domain; hence this process will be immune to the above mentioned sampling rate mismatch. The motion of the target over multiple PRIs is also taken into account in the development of the frequency-domain DBF algorithm to prevent performance degradation.

This paper is organized as follows. In Section II, the principles of a single receive channel circulating time-delay coded array and STCA will be briefly reviewed first. Then, the signal models of these two arrays under ultra-wideband circumstances will be developed, and a performance analysis of the time-domain DBF algorithm in such cases will be performed. The space code agility-based single channel DBF method for ultra-wideband radar will be presented in Section III. The signal model and low sidelobe principle of the space code agility-based space-time coded array (SCA-STCA) will then be introduced, followed by the frequency-domain DBF algorithm. Section IV concludes this paper.

II. PROBLEM FORMULATION

In this paper, it is assumed that an ultra-wideband signal with central frequency f_c and bandwidth B ($f_c \gg B$) is transmitted by a radar. Without loss of generality, the ultra-wideband transmit signal can be expressed as:

$$s_{\mathrm{T}}(t) = s_{\mathrm{B}}(t) \cdot e^{j2\pi f_c t} \tag{1}$$

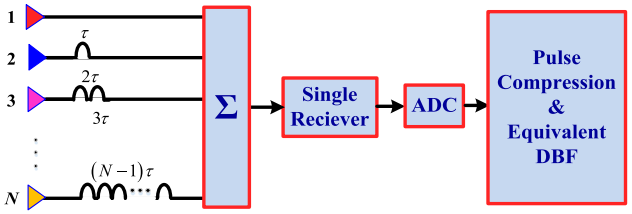

FIGURE 1. Architecture of a circulating time-delay coded array with a single receive channel.

where $s_{\mathrm{B}}(t)$ is the baseband signal with bandwidth B that can be either a linear frequency-modulated (LFM) signal or a phase-coded (PC) signal.

A. SIGNAL MODEL AND PERFORMANCE ANALYSIS OF A CIRCULATING TIME-DELAY CODED ARRAY RADAR UNDER ULTRA-WIDEBAND CIRCUMSTANCE

In the following, we will first review the architecture of a CTDCA [12]–[15]. Then, the CTDCA signal model under ultra-wideband circumstances will be developed, and a performance analysis of existing single-channel DBF methods under ultra-wideband circumstances will be conducted. For simplicity, a uniform linear array (ULA) consisting of N elements is employed for receiving. The element spacing is one-half of the wavelength. As shown in Figure 1, under the circulating time-delay coded array architecture, the received signals of the array elements are delayed by TTD lines with progressively increasing delay times. The delay time for the nth element is set to $(n-1)\tau$. Herein, τ is a constant. To avoid the coherent combination of these received signals, τ should satisfy $\tau \geq 1/B$. For simplicity, we assume $\tau = 1/B$ in this paper. After the delay operation, these received signals are summed together. Then, one can use a single receiver and a single ADC to record the combined signal.

Consider the returned signal from a point-like target with range R and impinging angle θ. The summation of all received signals of the array elements can be expressed as follows:

$$r(t,\theta) = \sigma_0 \cdot \sum_{n=1}^{N} s_{\mathrm{T}}\left(t - \frac{2R}{c} - (n-1)\cdot\tau(\theta)\right) \tag{2}$$

where $\sigma_0$is the complex amplitude of the returned signal, $\tau(\theta) = \tau + d\sin\theta/c$, d is the element spacing, $d = \lambda/2$ and λ is the wavelength.

Note that the spatial samples obtained by the array elements have been transformed into temporal sequential samples at this stage. Moreover, that the delay of the signal envelope introduced by the path difference between array elements is taken into account in (2), which is different from the signal models presented in Ref. [12]–[15]. The element spacing is comparable to the range resolution under ultra-wideband circumstances. Then, the delay of the signal envelope cannot be ignored in such cases. If this delay is ignored, the performance of the existing single channel DBF methods [12]–[15] with a CTDCA architecture will degrade, which will be discussed later in this subsection.

The baseband output signal of the single receiver will be recorded by an ADC. Then, the pulse compression operation will be carried out on the recorded signal. The output signal of the pulse compression process can be expressed as:

$$\begin{aligned} r_{\mathrm{c}}(t,\theta) &= \sigma_0 \cdot \sum_{n=1}^{N} s_{\mathrm{c}}\left(t - \frac{2R}{c} - (n-1)\cdot\tau(\theta)\right) \\ &\quad \cdot e^{-j2\pi f_c \cdot \left[\frac{2R}{c} + (n-1)\cdot\tau(\theta)\right]} \\ &= \sigma_0 \cdot e^{-j\frac{4\pi R}{\lambda}} \cdot s_{\mathrm{c}}\left(t - 2R/c\right) \\ &\quad * \left[\mathbf{a}(\tau(\theta))^T \boldsymbol{\delta}(\tau(\theta))\right] \end{aligned} \tag{3}$$

where "$*$" denotes convolution and $s_{\mathrm{c}}(t)$ represents the pulse compression output with respect to the transmit signal. For example, $s_{\mathrm{c}}(t)$ will be a sinc function if an LFM signal is transmitted. The half-power width of $s_{\mathrm{c}}(t)$ in the time domain equals $1/B$. $\mathbf{a}(\tau(\theta))$ and $\boldsymbol{\delta}(\tau(\theta))$ can be expressed as:

$$\mathbf{a}(\tau(\theta)) = \left[1, e^{-j2\pi f_c \cdot \tau(\theta)}, \cdots, e^{-j2\pi f_c \cdot (N-1)\cdot\tau(\theta)}\right]^T \tag{4}$$

$$\begin{aligned} \boldsymbol{\delta}(\tau(\theta)) = [&\delta(t), \delta(t - \tau(\theta)), \cdots, \delta(t - (N-1) \\ &\cdot\tau(\theta))]^T \end{aligned} \tag{5}$$

where $\delta(t)$ represents the impulse function. Obviously, $\boldsymbol{\delta}(\tau(\theta))$ is a sampling function. Let:

$$s_{\mathrm{st}}(t,\theta) = \mathbf{a}(\tau(\theta))^T \boldsymbol{\delta}(\tau(\theta)) \tag{6}$$

where $s_{\mathrm{st}}(t,\theta)$ is the space-time response function of the CTDCA. As shown in Figure 2, one can find that $s_{\mathrm{st}}(t,\theta)$ is a discrete sampling representation of the complex sinusoid signal $e^{-j2\pi f_c \cdot t}$. Denote the sampling rate of $s_{\mathrm{st}}(t,\theta)$ by $f_{\mathrm{SE}}(\theta)$. We have:

$$f_{\mathrm{SE}}(\theta) = 1/\tau(\theta) \tag{7}$$

One can find that the sampling rate of $s_{\mathrm{st}}(t,\theta)$ depends on the impinging angle of the returned signal. Returned signals from different angles will result in discrete complex sinusoid signals sampled with different sampling rates. Furthermore, since $\tau = 1/B \gg 1/f_c$, $f_{SE}(\theta)$ is much smaller than f_c. As a result, $s_{\mathrm{st}}(t,\theta)$ is actually an undersampled representation of $e^{-j2\pi f_c \cdot t}$. Therefore, $s_{\mathrm{st}}(t,\theta)$ is equivalent to the sampling representation of $e^{-j2\pi f_{am}(\theta)\cdot t}$. Herein, $f_{am}(\theta)$ is the folded ambiguous frequency of f_c under the sampling rate $f_{SE}(\theta)$. For example, consider a CTDCA consisting of 8 elements. The other array parameters are listed in TABLE 1. Figure 2 plots the resulting $s_{\mathrm{st}}(t,\theta)$ under two impinging angles $\theta_1 = -30°$ and $\theta_2 = -10°$. One can find that the returned signals from different angles result in time-domain discrete complex sinusoid signals with different frequencies. A time-domain bandpass filter should then be utilized to extract the signals from a given angle. Therefore, DBF can be accomplished through time-domain convolution based bandpass filtering instead of spatial filtering. This time-domain bandpass filter will be referred to as the time-domain equivalent DBF (EDBF) filter hereafter.

TABLE 1. Parameters of the array.

f_c	11 GHz	B	1.0 GHz	τ	1 ns	d	0.0136 m

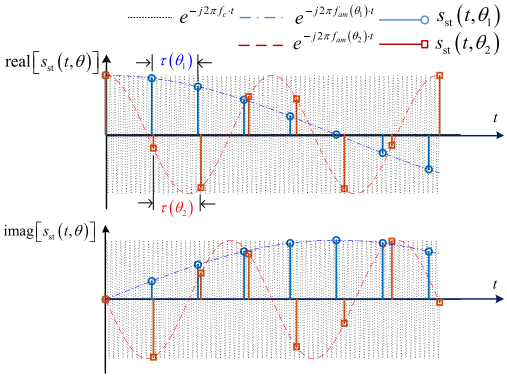

FIGURE 2. Demonstration of $s_{st}(t,\theta)$ when $N = 8$.

To form a receive beam pointing with an angle θ_0, the impulse response function of the time-domain EDBF filter is given by:

$$h(t,\theta_0) = s_{st}^{\dagger}(-t,\theta_0) = \mathbf{a}(\tau(\theta_0))^H \boldsymbol{\delta}(-\tau(\theta_0)) \tag{8}$$

where "$\dagger$" represents conjugation. Then, the EDBF output signal can be expressed as follows:

$$\begin{aligned} r_{\mathrm{EDBF}}(t,\theta_0) &= r_{\mathrm{c}}(t,\theta) * h(t,\theta_0) \\ &= \sigma_0 \cdot e^{-j4\pi R/\lambda} \cdot s_c\left(t - 2R/c\right) * \delta_{\mathrm{c}}(\theta,\theta_0) \end{aligned} \tag{9}$$

where

$$\begin{aligned} \delta_{\mathrm{c}}(\theta,\theta_0) &= s_{st}(t,\theta) * h(t,\theta_0) \\ &= \sum_{n=1}^{N}\sum_{m=1}^{N} e^{-j2\pi f_c \cdot (n-1)\cdot\tau(\theta)} \cdot e^{j2\pi f_c \cdot (m-1)\cdot\tau(\theta_0)} \\ &\quad \cdot\delta(t - (n-1)\cdot\tau(\theta) + (m-1)\cdot\tau(\theta_0)) \end{aligned} \tag{10}$$

In the case of $\theta = \theta_0$, $\delta_{\mathrm{c}}(\theta,\theta_0)$ can be rewritten as:

$$\begin{aligned} \delta_{\mathrm{c}}(\theta_0,\theta_0) = \sum_{l=-(N-1)}^{N-1} & e^{-j2\pi f_c \cdot l\cdot\tau(\theta_0)} \cdot (N - |l|) \\ & \cdot\delta(t - l\cdot\tau(\theta_0)) \end{aligned} \tag{11}$$

This means that some impulses of $\delta_{\mathrm{c}}(\theta,\theta_0)$ will overlap with each other. As shown in Figure 3, one can find that $\delta_{\mathrm{c}}(\theta_0,\theta_0)$ is actually a discrete triangular function with only $2N-1$ impulses. Herein, the array parameters are the same as Figure 2. Then, we have:

$$\begin{aligned} s_{\mathrm{c}}\left(t - 2R/c\right) * \delta_{\mathrm{c}}(\theta_0,\theta_0) = \sum_{l=-(N-1)}^{N-1} & e^{-j2\pi f_c \cdot l\cdot\tau(\theta_0)} \cdot (N - |l|) \\ & \cdot s_c\left(t - 2R/c - l\cdot\tau(\theta_0)\right) \end{aligned} \tag{12}$$

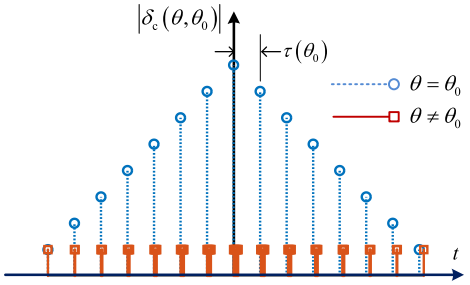

FIGURE 3. Demonstration of $\delta_c(\theta,\theta_0)$ when $N=8$.

One can find that the $2N-1$ scaled and delayed replicas of $s_c\left(t-2R/c\right)$ will have little impact on each other. Because the time interval between any two neighboring replicas is $\tau(\theta_0)$, which is around the mainlobe width of $s_c\left(t-2R/c\right)$, the maximum gain of the proposed EDBF process equals N, as with ordinary DBF.

In the case of $\theta \neq \theta_0$, the N^2 impulses of $\delta_c(\theta,\theta_0)$ are separated from each other in the time domain, as shown in Figure 3. These N^2 impulses can be divided into $2N-1$ groups. The phase difference between any two neighboring impulses in each group equals $e^{-j2\pi f_c\cdot d\cdot(\sin\theta-\sin\theta_0)/c}$, and the time difference between them equals $d\cdot(\sin\theta-\sin\theta_0)/c$, which is much smaller than the range resolution of $s_c(t)$. Therefore, the phase-shifted and delayed replicas of $s_c\left(t-2R/c\right)$ resulting from the impulses within a group will interfere with each other in a manner similar to the synthesis of far-field array signals. As a result, the magnitude of $r_{EDBF}(t,\theta_0)$ will be modulated by the pattern of the receive array with respect to the expected angle θ_0 and impinging angle θ. Therefore, spatial filtering (i.e., DBF) is accomplished.

Moreover, according to (12), one can find that the time-domain half-power width of $s_c\left(t-2R/c\right)*\delta_c(\theta_0,\theta_0)$ is $2\left(1-1/\sqrt{2}\right)N\cdot\tau(\theta_0)$. This means that the EDBF process will degrade the range resolution by a factor of $2\left(1-1/\sqrt{2}\right)N$. This is the cost of implementing DBF with a single receive channel through circulated time-delay receiving. The range resolution can be improved by the space-time coded technique, which will be discussed in the next subsection.

It should be noted that the time-domain EDBF process described by (9) will work normally only in the case that the sampling rate of the ADC is identical to a multiple of the sampling rate of $h(t,\theta_0)$, i.e., $Q\cdot f_{SE}(\theta_0)$. Herein, Q is a positive integer. However, $f_{SE}(\theta_0)$ will vary with the angle θ_0. Additionally, the sampling rate of ADC $f_{S\mathrm{ADC}}$ is usually fixed. For example, let $f_{S\mathrm{ADC}}=B=1/\tau$. In such a case, one can create an EDBF filter as follows:

$$h'(t,\theta_0)=\mathbf{a}(\tau(\theta_0))^H\boldsymbol{\delta}\left(-\tau'\right) \tag{13}$$

where $\tau'=round(\tau\cdot f_s)/f_s$, in which $round(\cdot)$ denotes the operation to obtain the integer nearest to the variable in the brace and f_s is the sampling rate of the ADC. The difference between the temporal widths of $h'(t,\theta_0)$ and $h(t,\theta_0)$ equals $(N-1)\cdot d\cdot\sin\theta_0/c$, which will increase with $|\theta_0|$. For ultra-wideband radar, $(N-1)\cdot d\cdot\sin\theta_0/c$ will be comparable to the time delay τ. Thus, the mismatch between $h'(t,\theta_0)$ and $h(t,\theta_0)$ is not negligible. Consequently, the performance of the discussed EDBF process will degrade.

TABLE 2. Parameters of the targets.

	Target 1	Target 2	Target 3	Target 4
Impinging Angle	0°	20°	40°	60°
Range	23750 m	23768 m	23786 m	23840 m
Velocity	55 m/s	70 m/s	90 m/s	115 m/s

To demonstrate this performance degradation, a CTDCA consisting of 63 elements is employed. The other parameters of this array are listed in TABLE 1. f_s is assumed to be 1.05 GHz, which is slightly larger than the bandwidth of the array. It is also assumed that there exist four equal-power targets with different impinging angles and ranges, which are listed in TABLE 2. The velocity of the target is neglected in this section since only one pulse is considered. One can find that the angular difference between any two targets is larger than the mainlobe beamwidth of the array and that the range difference between any two targets is larger than the degraded range resolution after the EDBF process. Therefore, these targets will appear in different receive beams and range resolution cells. Then, the EDBF algorithm described by (9) and (13) can be utilized to form receive beams with angles of 0°, 20°, 40° and 60°, through which the echoes of each target can be extracted. Figure 4 plots the simulation results of the pulse compression and EDBF process. As shown in Figure 4(a), the pulse compression results of signals from different impinging angles exhibit different frequencies. Moreover, as shown in Figure 4(b), the range resolution deteriorates to 5.5 m after the EDBF process. However, the range resolution corresponding to a 1 GHz bandwidth should be 0.15 m. One can further find that the gain in the EDBF process decreases with an increase in the impinging angle, which results from the sampling rate mismatch. Finally, the resulting beampatterns of the EDBF process with different beam pointing angles are plotted in Figure 4(c) and Figure 4(d). As one can see, the sidelobe nulls disappear from the resulting beampatterns, and the shape of the beampattern distorts significantly in the case of a large beam pointing angle due to the sampling rate mismatch.

B. SIGNAL MODEL AND PERFORMANCE ANALYSIS OF A SPACE-TIME CODED ARRAY RADAR UNDER ULTRA-WIDEBAND CIRCUMSTANCES

The array architecture discussed in the last subsection will result in a reduced range resolution. To preserve the range resolution, an STCA should be employed [16]. Such an array is developed for transmit DBF. However the principles of this array can also be utilized for receiving. The architecture of such an array is demonstrated in Figure 5. As one can see, a constant phase shifter is employed by each

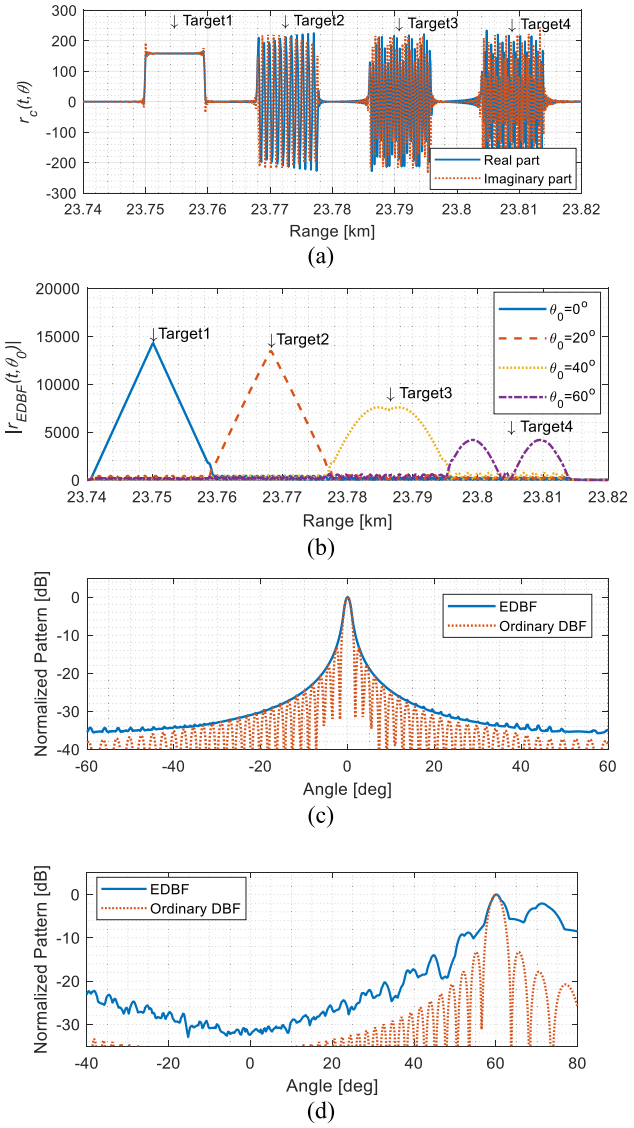

FIGURE 4. EDBF results of a circulating time-delay coded array with a single receive channel; (a) result of pulse compression; (b) results of EDBF; (c) receive beampattern with $\theta_0 = 0°$; (d) receive beampattern with $\theta_0 = 60°$.

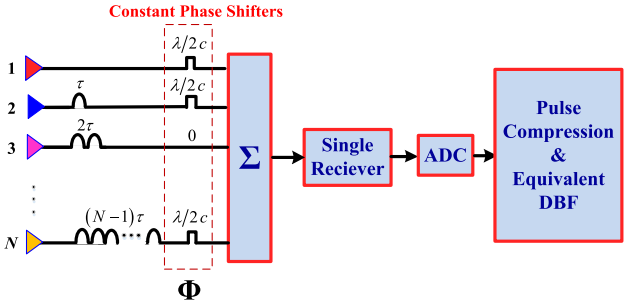

FIGURE 5. Architecture of single channel Space-time coded array with single receive channel.

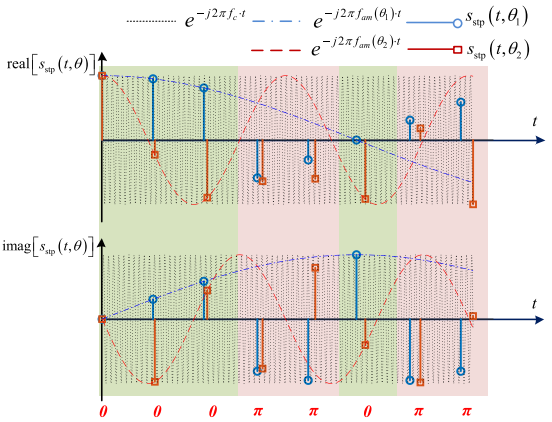

FIGURE 6. Demonstration of $s_{stp}(t, \theta)$.

receiving element. For simplicity, we consider constant phase shifters with phase shifts of 0 or π; in practice, such phase shifters can be implemented by a delay line with a length of 0 or $\lambda/2$, respectively. Therefore, the range compression output signal can be expressed as:

$$r_{cp}(t) = \sigma_0 \cdot e^{-j4\pi R/\lambda} \cdot s_c\left(t - 2R/c\right) * s_{stpc}(t, \theta) \quad (14)$$

where

$$s_{stp}(t, \theta) = \left[\mathbf{\Phi} \odot \mathbf{a}(\tau(\theta))\right]^T \boldsymbol{\delta}_p(\tau(\theta), \mathbf{\Phi}) \quad (15)$$

Herein, "$\odot$" represents the Hadamard product, $\mathbf{\Phi} = \left[e^{j\phi(1)}, e^{j\phi(2)}, \cdots, e^{j\phi(N)}\right]^T$ is a pseudorandom binary phase code vector, and $\phi(n)$ is the constant phase shift assigned to the nth element of the array. $\phi(n)$ can only be 0 or π. $\mathbf{\Phi}$ will be referred to as the space coding vector in this paper, and $\boldsymbol{\delta}_p(\tau(\theta), \mathbf{\Phi})$ is given by:

$$\boldsymbol{\delta}_p(\tau(\theta), \mathbf{\Phi}) = \begin{bmatrix} \delta\left(t - \lambda \cdot \phi(1)/(2\pi \cdot c)\right) \\ \delta\left(t - \tau(\theta) - \lambda \cdot \phi(2)/(2\pi \cdot c)\right) \\ \vdots \\ \delta\left(t - (N-1) \cdot \tau(\theta) - \lambda \cdot \phi(N)/(2\pi \cdot c)\right) \end{bmatrix} \quad (16)$$

where $s_{stp}(t, \theta)$ is the space-time response function of the STCA. Compared to $s_{st}(t, \theta)$, $s_{stp}(t, \theta)$ is a discrete phase-coded complex sinusoid signal, as shown by Figure 6 (wherein the array parameters are the same as those in Figure 2). Let:

$$\begin{aligned} h_p(t, \theta_0) &= s_{stp}^{\dagger}(-t, \theta_0) \\ &= \left[\mathbf{\Phi} \odot \mathbf{a}(\tau(\theta_0))\right]^H \boldsymbol{\delta}_p(-\tau(\theta_0), -\mathbf{\Phi}) \end{aligned} \quad (17)$$

The output signal of the EDBF process under the array architecture discussed in this section can be expressed as follows:

$$\begin{aligned} r_{EDBF}(t, \theta_0) &= r_{cp}(t) * h_p(t, \theta_0) \\ &= \sigma_0 \cdot e^{-j4\pi R/\lambda} \cdot s_c\left(t - 2R/c\right) * \delta_{cp}(\theta_0, \theta) \end{aligned} \quad (18)$$

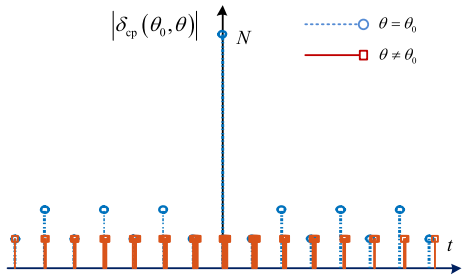

FIGURE 7. Demonstration of $\delta_{\mathrm{cp}}(\theta,\theta_0)$ when N=8.

where

$$\begin{aligned}\delta_{\mathrm{cp}}(\theta_0,\theta) &= s_{\mathrm{stp}}(t,\theta) * h_{\mathrm{p}}(t,\theta_0)\\ &\approx \sum_{n=1}^{N}\sum_{m=1}^{N} e^{-j2\pi f_c\cdot(n-1)\cdot\tau(\theta_k)}\\ &\quad\cdot e^{j2\pi f_c\cdot(m-1)\cdot\tau(\theta_0)}\cdot e^{j(\phi(m)-\phi(n))}\\ &\quad\cdot\delta\left(t-(n-1)\cdot\tau(\theta)+(m-1)\cdot\tau(\theta_0)\right.\\ &\quad\left.-\frac{\lambda\cdot(\phi(n)-\phi(m))}{2\pi\cdot c}\right)\end{aligned} \tag{19}$$

The possible values of $\lambda\cdot(\phi(n)-\phi(m))/(2\pi\cdot c)$ are $\lambda/2c$, 0 and $-\lambda/2c$. $f_c \gg B$, $\lambda/2c \ll 1/B$, and $\delta_{\mathrm{cp}}(\theta_0,\theta_0)$ can be approximated by the following:

$$\delta_{\mathrm{cp}}(\theta_0,\theta_0) \approx \sum_{l=-(N-1)}^{N-1} e^{-j2\pi f_c\cdot l\cdot\tau(\theta_0)}\cdot\delta(t-l\cdot\tau(\theta_0))\cdot\chi_{\mathbf{\Phi}}(l) \tag{20}$$

where

$$\chi_{\mathbf{\Phi}}(l)=\begin{cases}\sum_{q=1}^{N-l} e^{j(\phi(q+l)-\phi(q))}; & l\geq 0\\ \sum_{q=1}^{N-l} e^{j(\phi(q)-\phi(q-l))}; & l<0\end{cases} \tag{21}$$

Hence, one can find that $\chi_{\mathbf{\Phi}}(l)$ is the auto correlation function of the pseudorandom space coding vector $\mathbf{\Phi}$. $|\chi_{\mathbf{\Phi}}(l)|$ will reach its maximum when $l=0$ and drop sharply when $l\neq 0$. Therefore, the range resolution of $\delta_{\mathrm{cp}}(\theta_0,\theta_0)$ equals $\tau(\theta_0)$, as shown in Figure 7 (wherein the parameters are the same as those in Figure 3). Since $\tau=1/B \gg d/c$, the half-power width of $\delta_{\mathrm{cp}}(\theta_0,\theta_0)$ is approximately $1/B$. Therefore, the half-power width of $s_c(t-2R_k/c) * \delta_{\mathrm{cp}}(\theta_0,\theta_0)$ will remain almost $1/B$. This implies that the range resolution will be preserved under the array architecture discussed in this section.

The EDBF process described by (18) is in fact the match filter employed to coherently integrate the received signals from the expected angle. The match filter of a pseudorandom phase-coded signal is sensitive to the frequency shift. Since the returned signals from different angles will result in discrete phase-coded complex sinusoid signals with different frequencies, the match filtering operation will be sensitive to the impinging angle of the returned signal. In the case of $\theta_0\neq\theta$, the EDBF process is essentially equivalent to a mismatch filter for the pseudorandom phase-coded signal. Similarly, the maximum magnitude of the corresponding output will decrease with increasing $|\theta_0-\theta|$. Therefore, spatial filtering (i.e., DBF) is accomplished. However, the EDBF process described by (18) will also suffer from the mismatch between the sampling rates of the ADC and $h_{\mathrm{p}}(t,\theta_0)$.

Moreover, as is well known, for a pseudorandom phase-coded signal, the sidelobe level of the match filtering output is inversely proportional to the number of phase codes. The average output power of the mismatch filter is also inversely proportional to the number of phase codes. Therefore, under the array architecture discussed in this subsection, the sidelobe levels of the EDBF output in both the range domain and the angular-domain will be inversely proportional to the number of space codes, i.e., the number of array elements. For a very large-scale receive array, the resulting sidelobe levels will be acceptable; otherwise, the resulting sidelobe levels will be apparently higher than those of an ordinary array. However, for the array architecture discussed above, the number of array elements will be limited by the implementation of analog time-delay mechanisms. Therefore, it is necessary to find a way to reduce the sidelobe levels of the above mentioned array architecture without increasing the number of array elements. The solution to this problem will be discussed in the next section.

To demonstrate the range resolution preserving capability and the sidelobe degradation, an STCA with 63 elements is employed. An M-sequence code vector with a length of 63 is employed as the space coding vector. The other parameters of the array and targets are listed in TABLE 1 and TABLE 2, respectively. f_s is still assumed to be 1.05 GHz. The time-domain EDBF process described by (18) is employed to form receive beams with angles of 0°, 20°, 40° and 60°. Figure 8 plots the simulation results of the pulse compression and EDBF process. As shown in Figure 8(a), the pulse compression outputs are no longer single-frequency pulses due to the space coding. Moreover, as shown in Figure 8(b), the range resolution after the EDBF process is approximately 0.15 m, which is identical to that of a signal with a 1 GHz bandwidth. This proves that the range resolution is preserved. However, a range sidelobe, which is identical to that of an ordinary M-sequence coded signal, arises under the array architecture discussed in this subsection. The gain of the EDBF also degrades with an increase in the impinging angle. Figure 8(c) and Figure 8(d) plot the resulting beampatterns of the EDBF process. In addition to the observed pattern distortion, the angle sidelobe level increases significantly in the case of a large beam pointing angle.

III. SPACE CODE AGILITY BASED SINGLE CHANNEL DBF

As discussed above, the drawback of a CTDCA is the degradation of the range resolution, and the drawback of an STCA is the increased sidelobe levels in both the range and the angular domains. Moreover, the drawback of the time-domain

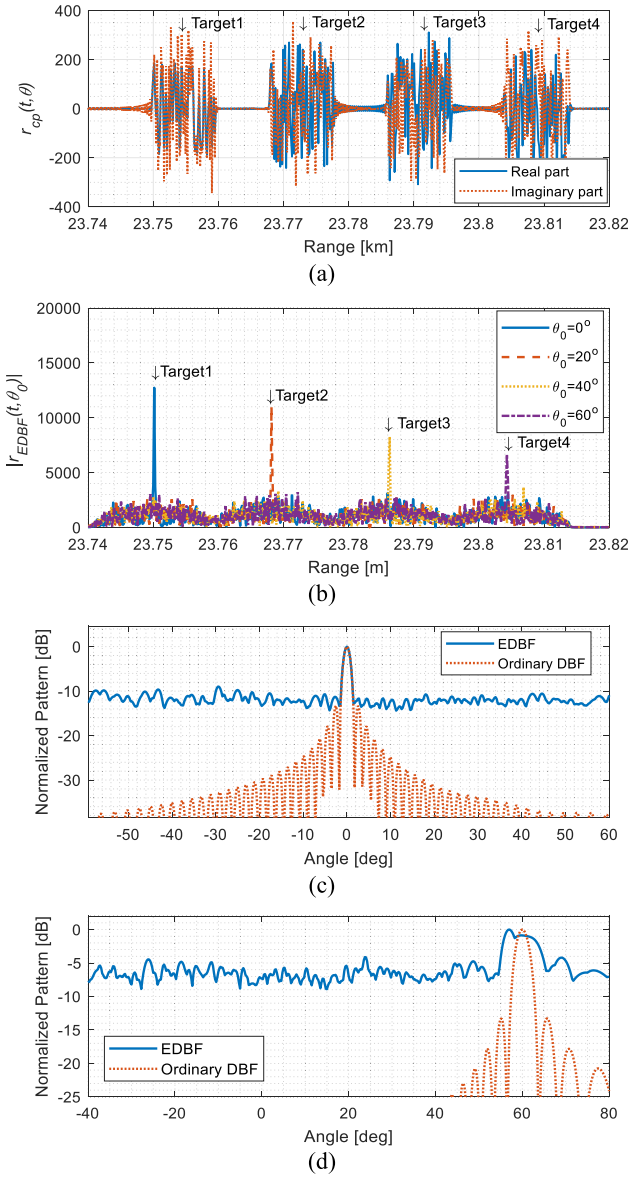

FIGURE 8. EDBF results of a space-time coded array with a single receive channel; (a) result of pulse compression; (b) results of EDBF; (c) receive beampattern with $\theta_0 = 0°$; (d) receive beampattern with $\theta_0 = 60°$.

convolution based EDBF algorithm is the performance degradation caused by the sampling rate mismatch. In this section, a new array architecture and a frequency-domain EDBF algorithm will be presented to overcome these problems.

A. ARRAY ARCHITECTURE AND LOW SIDELOBE EDBF PRINCIPLES

To reduce the sidelobe levels of an STCA with a single receive channel, the number of space codes must be increased. One feasible solution without increasing the number of array elements is to use irrelevant space coding vectors in different pulse repetition intervals (PRIs), i.e., space code agility. This is similar to the principle of synthetic aperture radar (SAR), which enlarges the aperture of the array by coherently integrating the signals received at different PRIs [18], [19].

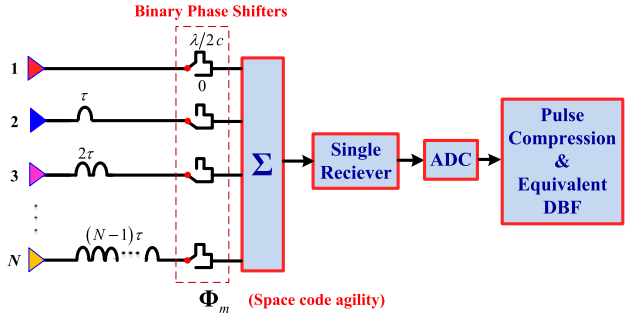

FIGURE 9. Architecture of a space-time coded array with space code agility.

Therefore, by coherently integrating signals received at multiple PRIs and modulated by irrelevant space coding vectors, the number of available space codes can be increased by a factor equal to the number of PRIs. Specifically, assume that there are M PRIs in each coherent processing interval (CPI). The total number of space codes will be enlarged by M times through space code agility. After coherently integrating the EDBF outputs of the M PRIs, the relative sidelobe levels in both the range domain and the angular domain can be decreased by a factor of M. From another point of view, for any two irrelevant phase-coded signals, their match filtering outputs will be independent, except the peak points. Therefore, the relative sidelobe levels can be reduced by coherently integrating the match filtering outputs of multiple irrelevant phase-coded signals. Similarly, the relative sidelobe levels of the EDBF output of an STCA can also be reduced by employing irrelevant space coding vectors in different PRIs.

The architecture of the space code agility-based space-time coded array (SCA-STCA) is demonstrated in Figure 9. Different from the architecture discussed in the last section, binary phase shifters are employed for the array elements. The phase shift of each element will remain constant within each PRI, and the phase shift will change from PRI to PRI. In such a case, the pulse compression output of the mth PRI can be expressed as:

$$r_{\mathrm{cpa}}(t,\theta,m) = \sigma_0 \cdot e^{\frac{-j4\pi R(m)}{\lambda}} \cdot s_c\left(t - 2R(m)/c\right) * s_{\mathrm{stpa}}(t,m,\theta) \quad (22)$$

where $R(m)$ is the target range in the mth PRI and $s_{\mathrm{stpa}}(t,m,\theta)$ is given by:

$$s_{\mathrm{stpa}}(t,m,\theta) = \left[\boldsymbol{\Phi}_m \odot \mathbf{a}(\tau(\theta))\right]^T \boldsymbol{\delta}_{\mathrm{p}}(\tau(\theta), \boldsymbol{\Phi}_m) \quad (23)$$

Herein, $\boldsymbol{\Phi}_m = \left[e^{\phi(1,m)}, e^{\phi(2,m)}, \cdots, e^{\phi(N,m)}\right]^T$ is the space coding vector of the mth PRI. We assume that $\boldsymbol{\Phi}_m$ and $\boldsymbol{\Phi}_k$ are irrelevant to each other when $m \neq k$. Let:

$$\begin{aligned} h_{\mathrm{pa}}(t,m,\theta_0) &= s^{\dagger}_{\mathrm{stpa}}(-t,m,\theta_0) \\ &= \left[\boldsymbol{\Phi}_m \odot \mathbf{a}(\tau(\theta_0))\right]^H \boldsymbol{\delta}_{\mathrm{p}}(-\tau(\theta_0), -\boldsymbol{\Phi}_m) \end{aligned} \quad (24)$$

For convenience, we first assume that $R(m)$ is a constant R_0. The time-domain EDBF process under the array architec-

ture proposed in this section can be expressed as follows:

$$\begin{aligned} r_{\text{EDBFPA}}(t,m,\theta,\theta_0) &= r_{\text{cpa}}(t,\theta,m) * h_{\text{pa}}(t,m,\theta_0) \\ &= \sigma_0 \cdot e^{-j\frac{4\pi R_0}{\lambda}} \cdot s_c\left(t-\frac{2R_0}{c}\right) \\ &\quad * \delta_{\text{cpa}}(\theta_0,\theta,m) \end{aligned} \tag{25}$$

where

$$\begin{aligned} \delta_{\text{cpa}}(\theta,\theta_0,m) \approx \sum_{k=1}^{N}\sum_{q=1}^{N} & e^{-j2\pi f_c\cdot(k-1)\cdot\tau(\theta)} \cdot e^{j2\pi f_c\cdot(q-1)\cdot\tau(\theta_0)} \\ & \cdot e^{j(\phi(k,m)-\phi(q,m))} \\ & \cdot \delta\left(t-(k-1)\cdot\tau(\theta)+(q-1)\cdot\tau(\theta_0)\right) \end{aligned} \tag{26}$$

To reduce the relative sidelobe levels, one must coherently integrate the EDBF outputs of the M PRIs. Let:

$$\begin{aligned} r_{\Sigma}(t,\theta,\theta_0) &= \sum_{m=1}^{M} r_{\text{EDBFPA}}(t,m,\theta,\theta_0) \\ &= \sigma_0 \cdot e^{-j4\pi R_0/\lambda} \cdot s_c\left(t-2R_0/c\right) * \delta_{\Sigma}(\theta,\theta_0) \end{aligned} \tag{27}$$

where

$$\begin{aligned} \delta_{\Sigma}(\theta,\theta_0) \approx \sum_{k=1}^{N}\sum_{q=1}^{N} & e^{-j2\pi f_c\cdot(k-1)\cdot\tau(\theta)} \cdot e^{j2\pi f_c\cdot(q-1)\cdot\tau(\theta_0)} \\ & \cdot \sum_{m=1}^{M} e^{j(\phi(k,m)-\phi(q,m))} \cdot \delta\left(t-(k-1)\right. \\ & \left.\cdot\tau(\theta)+(q-1)\cdot\tau(\theta_0)\right) \end{aligned} \tag{28}$$

One can find that $\delta_{\text{cpa}}(\theta,\theta_0,m)$ and $\delta_{\Sigma}(\theta,\theta_0)$ only differ in their space code terms, i.e., $e^{j(\phi(k,m)-\phi(q,m))}$ and $\sum_{m=1}^{M} e^{j(\phi(k,m)-\phi(q,m))}$. Since $\mathbf{\Phi}_m$ is a pseudorandom phase code vector, $e^{j\phi(k,m)}$ and $e^{j\phi(q,m)}$ can be regarded as irrelevant to each other when $k \neq q$.Then, the power of the space code term in $\delta_{\text{cpa}}(\theta,\theta_0,m)$ is given by:

$$\begin{aligned} & E\left|e^{j(\phi(k,m)-\phi(q,m))}\right|^2 \\ & \quad = E\left(e^{j(\phi(k,m)-\phi(q,m))}e^{-j(\phi(k,m)+\phi(q,m))}\right) = 1 \end{aligned} \tag{29}$$

where $E(\cdot)$ denotes the statistical average. Since $\mathbf{\Phi}_m$ and $\mathbf{\Phi}_k$ are assumed to be irrelevant to each other when $m \neq k$, the power of the space code term in $\delta_{\Sigma}(\theta,\theta_0)$ is given by:

$$\begin{aligned} & E\left|\sum_{m=1}^{M} e^{j(\phi(k,m)-\phi(q,m))}\right|^2 \\ & \quad = E\left(\sum_{m=1}^{M} e^{j(\phi(k,m)-\phi(q,m))}\sum_{u=1}^{M} e^{-j(\phi(k,u)+\phi(q,u))}\right) \\ & \quad = \sum_{\substack{m=1\\u=m}}^{M} E\left(e^{j(\phi(k,m)-\phi(q,m))}e^{-j(\phi(k,u)+\phi(q,u))}\right) \\ & \qquad + \sum_{m=1}^{M}\sum_{\substack{u=1\\u\neq m}}^{M} E\left(e^{j(\phi(k,m)-\phi(q,m))}e^{-j(\phi(k,u)+\phi(q,u))}\right) \\ & \quad = \begin{cases} M; & k \neq q \\ M^2; & k = q \end{cases} \end{aligned} \tag{30}$$

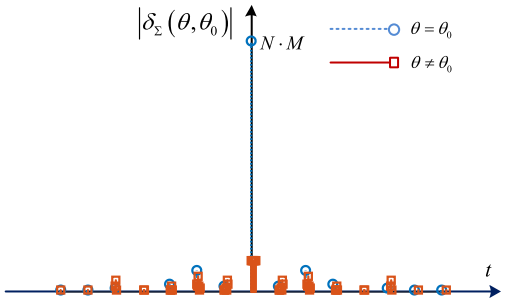

FIGURE 10. Demonstration of $\delta_{\Sigma}(\theta,\theta_0)$ when $N = 8$ and M=32.

The peaks of $\delta_{\text{cpa}}(\theta,\theta_0,m)$ and $\delta_{\Sigma}(\theta,\theta_0)$ will appear when $k = q$ and $\theta = \theta_0$. The peak power of $\delta_{\text{cpa}}(\theta,\theta_0,m)$ equals N^2, while the peak power of $\delta_{\Sigma}(\theta,\theta_0)$ equals $N^2 \cdot M^2$. The gain is M^2. However, the average sidelobe power of $\delta_{\text{cpa}}(\theta,\theta_0,m)$ equals 1, while the average sidelobe power of $r_{\Sigma}(t,\theta,\theta_0)$ equals M. Therefore, the relative sidelobe levels in both the range domain and the angular domain will be reduced by a factor of M.

Figure 10 plots the resulting $|\delta_{\Sigma}(\theta,\theta_0)|$ when $M = 32$ (the other parameters are the same as those in Figure 3). Compared with those plotted in Figure 7, the relative sidelobe levels are reduced significantly. One can further reduce the sidelobe levels by employing more PRIs with irrelevant space coding vectors.

Moreover, in most radar applications, the target of interest is not stationary; i.e., $R(m)$ is not a constant. The time-domain migration of the envelope of received signals during the M PRIs cannot be ignored in ultra-wideband cases. Therefore, in addition to the mismatch of the sampling rate, the performance of the time-domain convolution based EDBF process will also suffer from the motion of the target. In the next subsection, we will present an EDBF algorithm that can overcome the above problems through 2D frequency-domain processing.

B. FREQUENCY-DOMAIN EDBF ALGORITHM

Denote the velocity of a point-like target by v. Then, we have $R(m) = R_0 - (m-1)\cdot v\cdot T_r$, where T_r is the pulse repetition interval. Denote the baseband recorded signal of the SCA-STCA at the mth PRI by $r_{\text{pa}}(t,\theta,m)$. The spectrum of $r_{\text{pa}}(t,\theta,m)$ in the range frequency domain can be expressed as:

$$\begin{aligned} r_{\text{pa}}(f_r,\theta,m) = \sigma_0 \cdot S_B(f_r) \cdot e^{-j4\pi f_c\cdot R(m)/c} \cdot e^{-j4\pi f_r\cdot R(m)/c} \\ \cdot\left[\mathbf{A}(\tau(\theta),\mathbf{\Phi}_m)^T\,\mathbf{\Delta}(\tau(\theta),\mathbf{\Phi}_m)\right] \end{aligned} \tag{31}$$

where $S_B(f_r)$ is the spectrum of the transmit signal $s_B(t)$. $\mathbf{A}(\tau(\theta), \mathbf{\Phi}_m)$ and $\mathbf{\Delta}(\tau(\theta), \mathbf{\Phi}_m)$ can be expressed as:

$$\begin{aligned}&\mathbf{A}(\tau(\theta), \mathbf{\Phi}_m)\\&= \left[e^{-j2\pi f_c \cdot \frac{\lambda\cdot\phi(1,m)}{2\pi\cdot c}}, e^{-j2\pi f_c\cdot\left(\tau(\theta)+\frac{\lambda\cdot\phi(2,m)}{2\pi\cdot c}\right)},\right.\\&\left.\cdots, e^{-j2\pi f_c\cdot(N-1)\cdot\left(\tau(\theta)+\frac{\lambda\cdot\phi(N,m)}{2\pi\cdot c}\right)}\right]^T \qquad (32)\end{aligned}$$

$$\begin{aligned}&\mathbf{\Delta}(\tau(\theta), \mathbf{\Phi}_m)\\&= \left[e^{-j2\pi f_r \cdot \frac{\lambda\cdot\phi(1,m)}{2\pi\cdot c}}, e^{-j2\pi f_r\cdot\left(\tau(\theta)+\frac{\lambda\cdot\phi(2,m)}{2\pi\cdot c}\right)},\right.\\&\left.\cdots, e^{-j2\pi f_r\cdot(N-1)\cdot\left(\tau(\theta)+\frac{\lambda\cdot\phi(N,m)}{2\pi\cdot c}\right)}\right]^T \qquad (33)\end{aligned}$$

To coherently integrate the returned signals of M PRIs under ultra-wideband circumstances, the migration of the signal envelope resulting from the motion of the target should also be compensated. Specifically, the phase term $e^{-j4\pi f_r\cdot R(m)/c}$ should be removed from $r_{\text{pa}}(f_r, \theta, m)$. If v is known, it can be removed directly from the range frequency domain. However, v is usually unknown in practice. In such cases, the migration of the signal envelope can be corrected by using the Keystone transform. The details of the Keystone transform can be found in Ref. [20], [21], and thus, the specifics will not be further discussed in this paper. After applying Keystone transform, the spectrum of $r_{\text{pa}}(t, \theta, m)$ can be expressed as:

$$\begin{aligned}r'_{\text{pa}}(f_r, \theta, m) = \sigma_0 \cdot S_B(f_r) \cdot e^{-j4\pi f_c\cdot R(m)/c}\\ \cdot\left[\mathbf{A}(\tau(\theta), \mathbf{\Phi}_m)^T \mathbf{\Delta}(\tau(\theta), \mathbf{\Phi}_m)\right] \qquad (34)\end{aligned}$$

The Fourier transform of $h_{\text{pa}}(t, m, \theta_0)$ can be expressed as follows:

$$H_{\text{pa}}(f_r, m, \theta_0) = \mathbf{A}(\tau(\theta_0), \mathbf{\Phi}_m)^H \mathbf{\Delta}(-\tau(\theta_0), -\mathbf{\Phi}_m) \qquad (35)$$

One can find that $H_{\text{pa}}(f_r, m, \theta_0)$ can be precisely generated regardless of the practical sampling rate of the ADC. Therefore, the performance degradation resulting from the sampling rate mismatch can be avoided. Furthermore, range compression is usually accomplished in the frequency domain in practice. Therefore, receive beamforming can be accomplished with range compression simultaneously. The range and angle joint match filtering function can be expressed as:

$$H_{\text{J}}(f_r, m, \theta_0) = H_{\text{pa}}(f_r, m, \theta_0) \cdot S_B^{\dagger}(f_r) \qquad (36)$$

Moreover, before integrating the signals of M PRIs, the Doppler term $e^{-j4\pi f_c\cdot R(m)/c}$ should also be compensated, which can be achieved through a Doppler filter bank [24]. Then, the EDBF output in the kth Doppler channel can be expressed as follows:

$$\begin{aligned}r_{EDBF}(t, \theta_0, k) = \mathscr{F}^{-1}\left[\sum_{m=1}^{M} r'_{\text{pa}}(f_r, \theta, m)\right.\\ \left.\cdot H_{\text{J}}(f_r, m, \theta_0) \cdot e^{-j4\pi k\cdot\frac{F_r}{M}m\cdot T_r}\right] \qquad (37)\end{aligned}$$

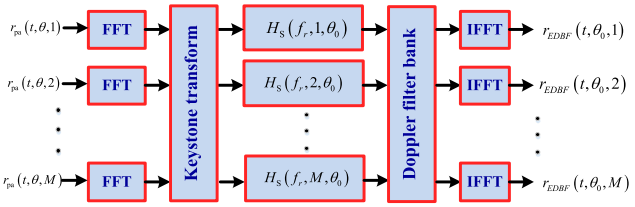

FIGURE 11. Signal processing workflow of the frequency-domain EDBF algorithm.

where F_r denotes the pulse repetition frequency, $T_r = 1/F_r$, and $\mathscr{F}^{-1}(\cdot)$ represents the inverse Fourier transform. The signal of the target will appear in the Doppler channel corresponding to its Doppler frequency. The signal processing workflow of the proposed frequency-domain EDBF approach is plotted in Figure 11, wherein $r_{\text{pa}}(t, \theta, m)$ denotes the output signal of the single receive channel in the mth PRI.

One should note that the range mainlobes of the target in the M PRIs will be coherently accumulated just at the Doppler channel corresponding to the Doppler frequency of the target according to (37). However, the range sidelobes cannot be coherently integrated since the range sidelobes of different PRIs are irrelevant. The energy of the range sidelobes will uniformly spread over the Doppler domain in a statistical sense. As a result, the Doppler sidelobe levels will be identical to the range sidelobe levels. However, as discussed before, the relative range sidelobe level of each target will be reduced by a factor of M through the proposed method. By increasing M, the relative Doppler sidelobe levels can also be reduced.

To demonstrate the effectiveness of the proposed array architecture and signal processing algorithm, we still consider a scene consisting of 4 targets with different ranges, impinging angles and velocities, and an STCA consisting of 63 elements is employed. The array parameters and target parameters are listed in TABLE 1 and TABLE 2, respectively. The velocities of these targets are different; hence, they should appear at different Doppler channels. Moreover, f_s is also assumed to be 1.05 GHz. For the convenience of the Doppler filtering process, we use 2^n PRIs within each CPI, where n is an integer. Moreover, 2^n irrelevant chaotic random binary phase code vectors [22], [23] are employed instead of the M-sequence code vector since the number of irrelevant M-sequence code vectors can be only $2^n - 1$.

Figure 12 plots the simulation results of the array architecture and signal processing procedure proposed in this section. Herein, $M = 64$. As shown in Figure 12(a)–(d), one can find that the four targets appear in different receive beams and Doppler channels due to their different impinging angles and velocities. More importantly, as shown in Figure 12(e), the range resolution is preserved while the sidelobe level is apparently improved compared with that plotted in Figure 8. Moreover, the peak of the target signal dose not degrade with an increase in the impinging angle. The slight variation in peak values is due to the mismatch between the center frequency of the Doppler filter and the Doppler frequency of

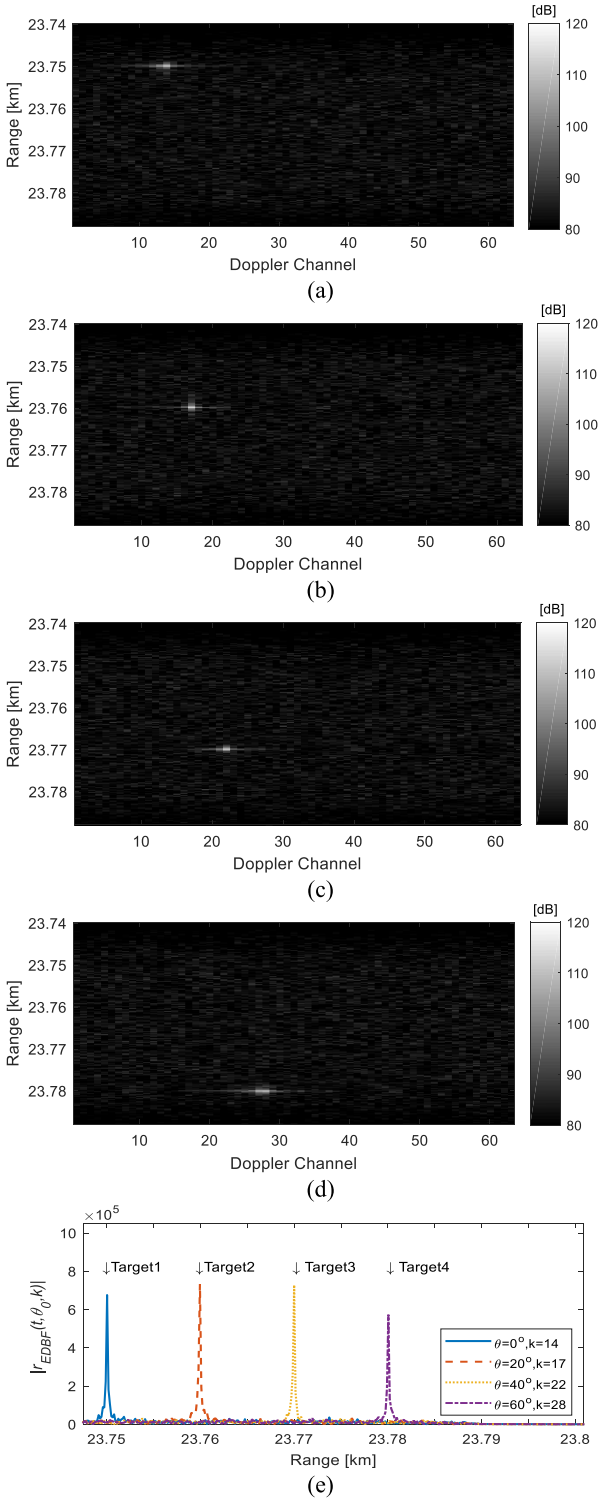

FIGURE 12. EDBF results of a space code-agility based space-time coded array with a single receive channel; (a) outputs of the Doppler filter bank when $\theta_0 = 0°$; (b) outputs of the Doppler filter bank when $\theta_0 = 20°$; (c) outputs of the Doppler filter bank when $\theta_0 = 40°$; (d) outputs of the Doppler filter bank when $\theta_0 = 60°$; (e) range profiles.

the target. This indicates that the proposed frequency-domain EDBF algorithm is immune to the sampling rate mismatch.

Figure 13(a) and Figure 13(b) plot the normalized receive beampatterns when different numbers of PRIs are utilized.

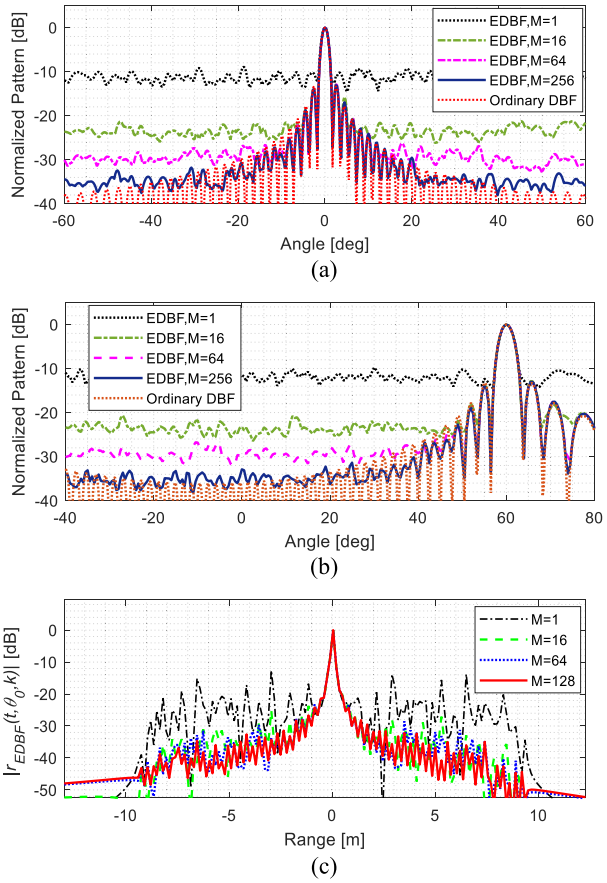

FIGURE 13. Normalized beampatterns and range profiles under different numbers of PRIs. (a) Receive beampatterns with $\theta_0 = 0°$; (b) receive beampatterns with $\theta_0 = 60°$; (c) normalized range profiles.

The sidelobe level in the angular domain decrease when only 16 PRIs are employed. The sidelobe level in this case will approach that with the ordinary DBF when $M = 256$. Moreover, the beampattern does not distort in the case of a large beam pointing angle. Figure 13(c) plots the normalized range profile of target 1. Similarly, the sidelobe level in the range domain also decreases with an increasing PRI number. However, the number of PRIs available will be limited by the motion of the target and the processing capability of the radar. One must compromise between the sidelobe levels and the above limitations.

In TABLE 3, the DBF quality parameters of the proposed SCA-STCA and the frequency-domain EDBF algorithm are compared with those of the CTDCA, STCA and time-domain EDBF algorithm. It should be noted that the mainlobe width of an ordinary array is utilized to calculate the angular peak sidelobe ratio (PSLR) and integrated sidelobe ratio (ISLR) of the CTDCA since the sidelobe nulls of the CTDCA disappear. One can find that the angular sidelobe level of the proposed SCA-STCA is closest to that of the ordinary digital array. The range sidelobe level of the SCA-STCA is even better than that of the ordinary LFM signal without the windowing process. In addition, the range resolution of the SCA-STCA is identical to that of the ordinary digital array and STCA. Moreover, the performance of the frequency-domain EDBF

TABLE 3. Performance comparison.

	θ_0	Ordinary array	CTDCA with time-domain EDBF [12]	STCA with time-domain EDBF [17]	SCA-STCA with frequency-domain EDBF (M=256)
PSLR (angular)	0°	-13.3 dB	-9.82 dB	-9.05 dB	-13.2 dB
	60°	-13.3 dB	-2.12 dB	-4.55 dB	-13.2 dB
ISLR (angular)	0°	-9.66 dB	-6.97 dB	6.41 dB	-9.49 dB
	60°	-9.89 dB	-2.11 dB	6.87 dB	-9.73 dB
PSLR (range)	0°	-13.3 dB	-59.51 dB	-14.61 dB	-21.28 dB
	60°	-13.3 dB	-50.23 dB	-6.97 dB	-25.81 dB
ISLR (range)	0°	-9.66 dB	-24.38 dB	10.39 dB	-15.57 dB
	60°	-9.66 dB	-9.54 dB	12.65 dB	-15.76 dB
Range resolution		0.15 m	5.5 m	0.15 m	0.15 m

algorithm does not degrade with an increasing beam pointing angle.

In summary, the proposed SCA-STCA and frequency-domain EDBF algorithm outperform the existing array architectures and algorithms.

IV. CONCLUSION

In this paper, a space code agility-based single channel DBF method for ultra-wideband radar was proposed. Compared to the single-channel EDBF of a circulating time-delay coded array, the range resolution of an ultra-wideband signal can be preserved through the proposed array architecture. Moreover, by using the received signals of multiple PRIs for DBF and changing the space code from PRI to PRI, the relative sidelobe levels in both the range and the angular domains can be reduced significantly, compared to the existing EDBF method with a space-time coded array. A frequency-domain equivalent DBF algorithm is developed that is immune to the mismatch between the sampling rate of the recorded signal and the space-time response function of the space-time coded array under ultra-wideband circumstances. The target motion is also taken into account in the development of the frequency-domain DBF algorithm. Numerical simulations verify the effectiveness of the proposed method.

REFERENCES

[1] H. Steyskal, "Digital beamforming antennas—An introduction," *Microw. J.*, vol. 30, pp. 107–110, Jan. 1986.
[2] J. D. Fredrick, Y. Wang, and T. Itoh, "A smart antenna receiver array using a single RF channel and digital beamforming," *IEEE Trans. Microw. Theory Techn.*, vol. 50, no. 12, pp. 3052–3058, Dec. 2002.
[3] J. D. Fredrick, Y. Wang, and T. Itoh, "Smart antennas based on spatial multiplexing of local elements (SMILE) for mutual coupling reduction," *IEEE Trans. Antnnas Propag.*, vol. 52, no. 1, pp. 106–114, Jan. 2004.
[4] S. Farzaneh and A. R. Sebak, "Microwave sampling beamformer—Prototype verification and switch design," *IEEE Trans. Microw. Theory Techn.*, vol. 57, no. 1, pp. 36–44, Jan. 2009.
[5] S. Kim and Y. E. Wang, "Two-dimensional planar array for digital beamforming and direction-of-arrival estimations," *IEEE Trans. Veh. Technol.*, vol. 58, no. 7, pp. 3137–3144, Sep. 2009.
[6] S. Henault, B. R. Jackson, and Y. M. M. Antar, "Compensation of time-division multiplexing distortion in switched antenna arrays with a single RF front-end and digitizer," *IEEE Trans. Antennas Propag.*, vol. 61, no. 8, pp. 4383–4388, Aug. 2013.
[7] C. Cui, D. Zhang, J. Zhang, and W. Wu, "A novel single RF channel scheme for smart antenna based on optical delay lines," in *Proc. 9th IEEE Asia–Pacific Microw. Photon. Conf.*, Sendai, Japan, Oct. 2014, pp. 204–207.
[8] W.-X. Sheng and D.-G. Fang, "Angular superresolution for phased antenna array by phase weighting," *IEEE Trans. Aerosp. Electron. Syst.*, vol. 37, no. 4, pp. 1450–1814, Oct. 2001.
[9] J. Zhang, W. Wu, and D. G. Fang, "Single RF channel digital beamforming multibeam antenna array based on time sequence phase weighting," *IEEE Antennas Wireless Propag. Lett.*, vol. 10, pp. 514–516, May 2011.
[10] E. A. Alwan, S. B. Venkatakrishnan, A. A. Akhiyat, W. Khalil, and J. L. Volakis, "Code optimization for a code-modulated RF front end," *IEEE Access*, vol. 3, pp. 260–273, Apr. 2015.
[11] D. Zhang, J. Zhang, C. Cui, W. Wu, and D. Fang, "Single RF channel digital beamforming array antenna based on compressed sensing for large-scale antenna applications," *IEEE Access*, vol. 6, pp. 4340–4351, 2018.
[12] G. Babur, G. O. Manokhin, A. A. Geltser, and A. A. Shibelgut, "Low-cost digital beamforming on receive in phased array radar," *IEEE Trans. Aerosp. Electron. Syst.*, vol. 53, no. 3, pp. 1355–1364, Jun. 2017.
[13] G. Babur, P. Aubry, and F. Le Chevalier, "Space-time radar waveforms: Circulating codes," *J. Elect. Comput. Eng.*, vol. 2013, pp. 261–268, Aug. 2013.
[14] S. Li, L. Zhang, N. Liu, J. Zhang, and S. Tang, "Transmit diversity technique based on joint slow-time coding with circulating code," *IET Radar, Sonar Navigat.*, vol. 11, no. 8, pp. 1243–1250, Aug. 2017.
[15] S. Li, L. Zhang, N. Liu, J. Zhang, S. Tang, and X. Huang, "Transmit beampattern synthesis for MIMO radar using extended circulating code," *IET Radar, Sonar Navigat.*, vol. 12, no. 6, pp. 610–616, Jun. 2018.
[16] G. Babur, P. Aubry, and F. L. Chevalier, "Simple transmit diversity technique for phased array radar," *IET Radar, Sonar Navigat.*, vol. 10, no. 6, pp. 1046–1056, 2016.
[17] L. Lan, G. Liao, J. Xu, S. Zhu, and Z. Wang, "Subarray-based time-delay low sidelobes methods for space-time coding array," *IET Radar, Sonar Navigat.*, vol. 12, no. 8, pp. 807–814, Aug. 2018.
[18] R. K. Raney, H. Runge, R. Bamler, I. G. Cumming, and F. H. Wong, "Precision SAR processing using chirp scaling," *IEEE Trans. Geosci. Remote Sens.*, vol. 32, no. 4, pp. 786–799, Jul. 1994.
[19] I. G. Cumming and F. H. Wong, *Digital Processing of Synthetic Aperture Radar Data: Algorithms and Implementation*. Norwood, MA, USA: Artech House, 2005, pp. 88–92.
[20] J. Zheng, J. Zhang, S. Xu, H. Liu, and Q. H. Liu, "Radar detection and motion parameters estimation of maneuvering target based on the extended keystone transform," *IEEE Access*, vol. 6, pp. 76060–76073, 2018.
[21] P. Huang, G. Liao, Z. Yang, X.-G. Xia, J.-T. Ma, and J. Ma, "Long-time coherent integration for weak maneuvering target detection and high-order motion parameter estimation based on keystone transform," *IEEE Trans. Signal Process.*, vol. 64, no. 15, pp. 4013–4026, Aug. 2016.
[22] S. Hong, F. Zhou, Y. Dong, Z. Zhao, Y. Wang, and M. Yan, "Chaotic phase-coded waveforms with space-time complementary coding for MIMO radar applications," *IEEE Access*, vol. 6, pp. 42066–42083, 2018.
[23] D. Shen, L.-R. Zhang, X. Liu, and N. Liu, "A novel method of using chaotic sequences in MIMO radar for multiple targets detection," in *Proc. IEEE 14th Int. Conf. Commun. Technol. (ICCT)*, Nov. 2012, pp. 914–918.
[24] G. W. Stimson, *Introduction to Airborne Radar*, 2nd ed. Raleigh, NC, USA: SciTech, 1998, pp. 477–485.

LIU NAN received the Ph.D. degree from Xidian University, Xi'an, China, in 2009. He is currently an Associate Professor with the National Laboratory of Radar Signal Processing, Xidian University. His current research interests include array signal processing, MIMO radar, and radar imaging.

GUO KAISI received the B.S. degree in electronic engineering from Xidian University, Xi'an, China, in 2017, where she is currently pursuing the M.S. degree in signal and information processing.

ZHANG ZHENGHE received the B.S. degree in electronic engineering and the M.S. degree in signal and information processing from Xidian University, Xi'an, China, in 2016 and 2019, respectively, where he is currently pursuing the Ph.D. degree in signal and information processing. His current research interests include array signal processing and MIMO radar.

ZHANG LINRANG received the M.S. and Ph.D. degrees from Xidian University, Xi'an, China, in 1991 and 1999, respectively. He is currently a Full Professor with the National Laboratory of Radar Signal Processing, Xidian University. His current research interests include radar signal processing, array signal processing, radar electronic counter-countermeasure, and radar imaging.